ANALYSIS OF SINGLE PILE ULTIMATE LATERAL RESISTANCE IN CLAYEY SOIL UNDER HORIZONTAL GROUND MOVEMENT USING RPFEM

Pham Ngoc Quang*, Pham Ngoc Vinh, Hoang Phuong Hoa

The University of Danang - University of Science and Technology, Vietnam

*Corresponding author: pnquang@dut.udn.vn

(Received: February 01, 2025; Revised: March 23, 2025; Accepted: March 26, 2025)

DOI: 10.31130/ud-jst.2025.23(6A).036E

Abstract - This study investigates the ultimate lateral resistance of a single pile subjected to horizontal ground movement in clayey soils, employing a self-developed Rigid Plastic Finite Element Method (RPFEM). The analysis effectively predicts the ultimate lateral resistance of a single pile by modeling the interaction between the pile and surrounding soil, with a focus on understanding the failure zones and overall resistance behavior. A key finding of this research is the critical influence of installation-induced strength reduction in the surrounding soil, which significantly impacts the ultimate lateral resistance of the pile. The results demonstrate a high sensitivity of lateral resistance to changes in soil strength caused by the pile installation process. These findings underscore the importance of incorporating such installation effects into geotechnical design assessments, as they are essential for improving the accuracy of pile behavior predictions, particularly in sensitive and clayey soil environments where soil strength changes are pronounced.

Key words – Ultimate lateral resistance; Single pile; Horizontal ground movement; Rigid plastic finite element method (RPFEM).

1. Introduction

Pile foundations play a crucial role in geotechnical engineering, supporting vertical loads while resisting horizontal forces and bending moments. This is especially important in earthquake-prone areas, where structural stability depends on accurately predicting the ultimate lateral resistance of a pile. However, despite various predictive methods [1–8], significant discrepancies remain between calculated and observed lateral resistance. These differences often stem from traditional linear elastic models, which fail to capture the complex, nonlinear behavior of soil under lateral loading.

The ultimate lateral resistance of a single pile, defined as its maximum horizontal load capacity, is crucial in pile foundation design. This resistance primarily depends on the interaction pressure between the pile and surrounding soil (p_u). Broms [1] proposed methods to estimate p_u for cohesive and cohesionless soils, originally for active piles but often applied to passive piles. For short piles in cohesive soils, he suggested calculating p_u from the ground surface to a depth of $1.5D$ (D = pile diameter or width), with values ranging from $8.28c_u$ to $12.56c_u$, where c_u is the undrained shear strength.

Randolph and Houlsby [2] later refined these estimates using classical plasticity theory for circular piles in cohesive soils. Their analysis applied both lower-bound (equilibrium stress distribution) and upper-bound (energy dissipation) approaches. For perfectly rough piles, they found p_u values between $9.14c_u$ and $11.94c_u$, improving the accuracy of lateral resistance predictions.

Pile installation in cohesive soils often leads to strength degradation due to remolding and displacement effects [6–8]. The extent of this degradation depends significantly on the installation method. Driven piles induce remolding and displacement, increasing pore water pressure and reducing effective stress, which leads to shear strength loss extending several pile diameters. Over time, consolidation may facilitate partial strength recovery. Bored piles, in contrast, reduce in-situ lateral stresses, causing stress relaxation and potential softening, further exacerbated by exposure to drilling fluids. Unlike driven piles, they do not benefit from soil densification, and strength recovery primarily depends on soil reconsolidation. Given these effects, a parametric sensitivity analysis is essential to quantify degradation and optimize installation techniques for improved foundation performance.

To address these issues, this study employs self-developed Finite Element Method (FEM) simulations to evaluate the ultimate lateral resistance of single piles and their behavior under lateral ground movement in clayey soils. The analysis uses the Rigid Plastic Finite Element Method (RPFEM), based on the upper-bound theorem of limit analysis. Originally developed by Tamura et al. [9] and later extended to frictional materials [10], RPFEM is widely used in geotechnical engineering to assess soil-structure stability. Its key advantage is the ability to calculate limit loads without predefined failure mode assumptions, making it highly effective for analyzing lateral resistance.

An in-house RPFEM code [11–24] was used for 2D analyses in the horizontal plane under static loading. These simulations provide detailed insights into pile-soil interactions, enabling accurate predictions of lateral resistance in clayey soils. The results were validated against Broms' slip-line solutions, confirming the model's accuracy and its potential for practical applications, including seismic design in geotechnical engineering.

2. Methodology for ultimate lateral resistance of pile

2.1. Rigid plastic constitutive equation for pile-soil system

The RPFEM is an analytical method that applies the upper bound theorem of limit analysis to finite element methods [11-24]. However, since the upper bound theorem is based on the associated flow rule, this limits the scope of its application. Tamura et al. [9 - 10] developed an equivalent rigid plastic constitutive relationship to the upper bound theorem. By applying rigid plastic theory in the form of constitutive equations, it is possible to construct

constitutive relationships without the constraints of the associated flow rule, which holds significant practical value for applications.

Drucker-Prager yield function was expressed using the first invariant of stress $I_1 = tr(\sigma_{ij})$ and the second invariant of the deviatoric stress $J_2 = \frac{1}{2}(s_{ij}s_{ij})$ as follows:

$$f(\boldsymbol{\sigma}) = \alpha I_1 + \sqrt{J_2} - k = 0 \tag{1}$$

in which, $\alpha = \frac{\tan\phi}{\sqrt{9+12\tan^2\phi}}$ and $k = \frac{3c}{\sqrt{9+12\tan^2\phi}}$ are coefficients associated with c and ϕ based on the Mohr-Coulomb failure criterion. The stress in a body undergoing plastic deformation is decomposed into a determinate stress $\boldsymbol{\sigma}^{(1)} = \boldsymbol{\sigma}_{ij}^{(1)}$, which can be obtained from the plastic strain rate, and an indeterminate stress $\boldsymbol{\sigma}^{(2)} = \boldsymbol{\sigma}_{ij}^{(2)}$, which cannot be derived from the plastic strain rate, as shown in Figure 1. The determinate stress, based on the associated flow rule, is expressed as follows. In the equation, $\dot{\boldsymbol{\varepsilon}} = \dot{\varepsilon}_{ij}$ denotes the plastic strain rate, and $\dot{e} = \sqrt{(\dot{\boldsymbol{\varepsilon}} : \dot{\boldsymbol{\varepsilon}})} = \sqrt{\dot{\varepsilon}_{ij}\dot{\varepsilon}_{ij}}$ represents the equivalent plastic strain rate.

$$\boldsymbol{\sigma}^{(1)} = \frac{k}{\sqrt{3\alpha^2+1/2}}\frac{\dot{\boldsymbol{\varepsilon}}}{\dot{e}} \tag{2}$$

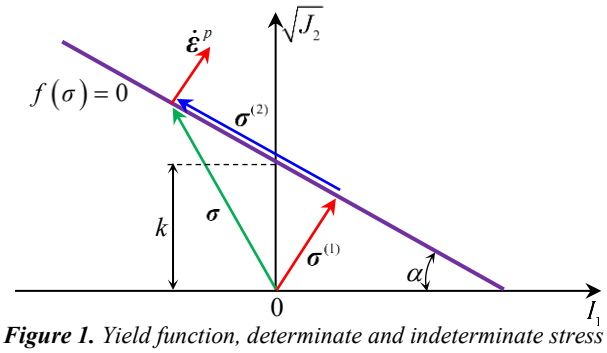

Figure 1. *Yield function, determinate and indeterminate stress*

The indeterminate stress cannot be directly obtained from the yield function. However, by utilizing the fact that the stress lies on the yield function, the components of the indeterminate stress (indefinite stress) can be defined. When the associated flow rule is applied to the yield function, a condition equation for the plastic strain rate (dilatancy characteristic) is derived.

$$h(\dot{\boldsymbol{\varepsilon}}) = \dot{\varepsilon}_v - \frac{3\alpha}{\sqrt{3\alpha^2+1/2}}\dot{e} = \dot{\varepsilon}_v - \beta\dot{e} = 0 \tag{3}$$

where, $\dot{\varepsilon}_v$ and $\dot{e}$ indicate the volumetric strain rate and the norm of the strain rate, respectively. By taking advantage of the fact that the above equation is orthogonal to the yield function, the indeterminate stress can be expressed as follows using an arbitrary constant λ.

$$\boldsymbol{\sigma}^{(2)} = \lambda\frac{\partial h}{\partial \dot{\boldsymbol{\varepsilon}}} = \lambda\left(\boldsymbol{I} - \frac{3\alpha}{\sqrt{3\alpha^2+1/2}}\frac{\dot{\boldsymbol{\varepsilon}}}{\dot{e}}\right) \tag{4}$$

where, $\boldsymbol{I}$ represents the unit tensor. Therefore, the rigid plastic constitutive equation for the Drucker-Prager yield function can be expressed as follows.

$$\boldsymbol{\sigma} = \boldsymbol{\sigma}^{(1)} + \boldsymbol{\sigma}^{(2)} = \frac{k-3\alpha\lambda}{\sqrt{3\alpha^2+1/2}}\frac{\dot{\boldsymbol{\varepsilon}}}{\dot{e}} + \lambda\boldsymbol{I} \tag{5}$$

This constitutive equation includes an arbitrary constant λ, which can be determined by conducting an analysis of boundary value problems along with the dilatancy characteristics (condition equations) concerning the plastic strain rate.

Since the rigid plastic constitutive equation applies to deformed bodies, it is fundamentally not applicable to rigid bodies. However, for stability analysis, it is necessary to include rigid body considerations. Therefore, the rigid plastic constitutive equation is extended as follows: if the equivalent plastic strain rate $\dot{e}$ falls below a threshold $\dot{e}_o$, the operation of replacing $\dot{e}$ with $\dot{e}_o$ is performed, resulting in the following equation.

$$\boldsymbol{\sigma} = \frac{k-3\alpha\lambda}{\sqrt{3\alpha^2+1/2}}\frac{\dot{\boldsymbol{\varepsilon}}}{\dot{e}} + \lambda\boldsymbol{I} = \frac{k-3\alpha\lambda}{\sqrt{3\alpha^2+1/2}}\frac{\dot{e}}{\dot{e}_o}\frac{\dot{\boldsymbol{\varepsilon}}}{\dot{e}} + \lambda\boldsymbol{I}$$
$$If\ \dot{e} \le \dot{e}_o \tag{6}$$

This corresponds to the operation of reducing the yield function by $\dot{e}/\dot{e}_o$, allowing for a small amount of plastic deformation in the rigid body portion, thereby constructing a constitutive relationship for the stress within the yield function that is similar to that of a plastic body. In this study, a method is employed to explicitly address the constraints using a penalty approach to accelerate the analysis speed (κ: penalty constant) [11-24]. Thus, the rigid plastic constitutive equation is ultimately given by the following equation.

$$\boldsymbol{\sigma} = \frac{k}{\sqrt{3\alpha^2+1/2}}\frac{\dot{\boldsymbol{\varepsilon}}}{\dot{e}} + \kappa(\dot{\varepsilon}_v - \beta\dot{e})\left(\boldsymbol{I} - \frac{3\alpha}{\sqrt{3\alpha^2+1/2}}\frac{\dot{\boldsymbol{\varepsilon}}}{\dot{e}}\right) \tag{7}$$

2.2. Ultimate lateral resistance of a single pile

This study examines the behavior of a single pile in a pile-soil system using the RPFEM under plane strain conditions, focusing on its ultimate lateral resistance. RPFEM's rigid plastic model eliminates uncertainties associated with the elastic modulus, a key limitation of conventional elastoplastic models. By accurately capturing pile-soil interactions, RPFEM provides precise deformation assessments, offering deeper insights into pile response under loading. Proper boundary condition definition is crucial, as discrepancies between the numerical model and real conditions can significantly affect the strain distribution and deformation behavior of a single pile.

The pile is modeled with high-strength solid elements, while the surrounding soil is represented by softer elements to reflect material variability. A static, uniform distribution load is incrementally applied until the pile reaches its ultimate lateral resistance p_u, as shown in Figure 2. The model includes detailed boundary conditions, with rigid outer boundaries simulating soil confinement and fixed support conditions at the pile's center to represent its rigid lateral load response, consistent with pile-soil interaction.

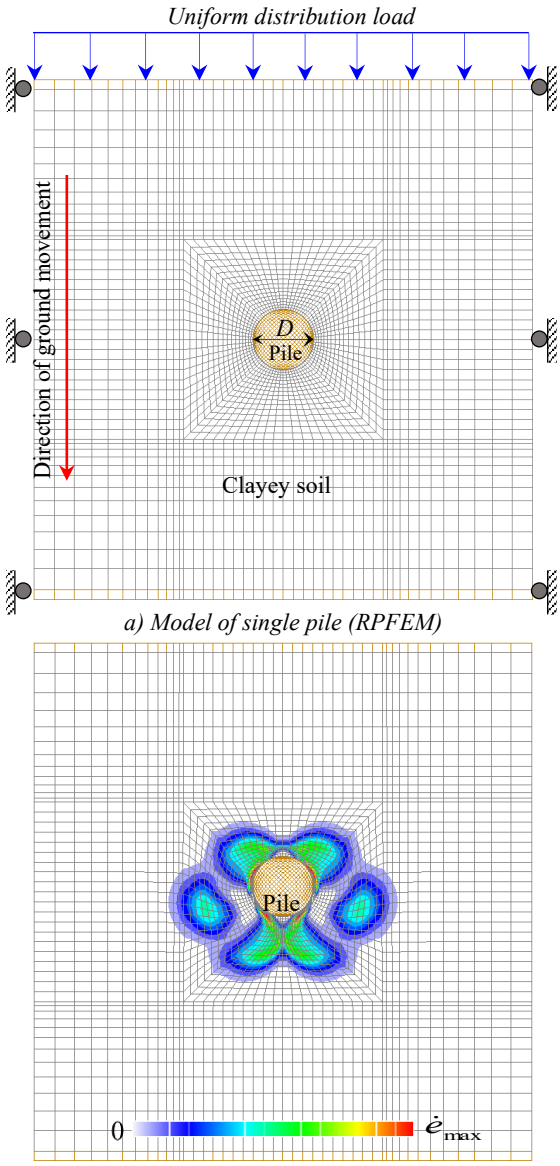

a) Model of single pile (RPFEM)

b) Failure mechanism of single pile (p_u=12.27c_u)

***Figure 2**. Typical finite element mesh and boundary conditions for a single pile modeled with RPFEM*

In the RPFEM constitutive model, the soil and pile materials are assumed to be perfectly plastic. The soil has an undrained shear strength of c_u=100 kPa and an internal friction angle of ϕ_s=0°, representing cohesive soils under undrained conditions [25-30]. The pile material is modeled with a large shear strength of c_p=50,000 kPa and ϕ_p=0°, to simulate a rigid pile, as shown in Table 1. The pile diameter is set at D=0.6 m, ensuring practical relevance and compatibility with the surrounding soil domain.

***Table 1.** Parameters for soil and pile parameters*

Parameters	Clayey soil	Single pile
Cohesive strength c [kPa]	100	50,000
Internal friction angle ϕ [°]	0	0

The ultimate lateral resistance of a single pile in clayey soil was calculated by RPFEM. The results illustrate a velocity field, as shown in Figure 2b, which indicates the failure mode around the pile. The strain rate norm is depicted by contour lines in the range of $\dot{e}_{max} \sim \dot{e}_{min}(0)$, highlighting variations in pile-soil interaction. The observed failure mode in the surrounding soil extends from approximately 1.5D to 2.0D from the pile's center, consistent with the slip-line pattern of Broms [1]. The calculated ultimate lateral resistance for the single pile was approximately p_u=12.27c_u, closely matching Broms' result of 12.56c_u. This value also shows good agreement with the findings of Georgiadis [25–27] (11.95c_u) and Zhao [28]. The small difference (less than 3%) indicates that the proposed approach provides a reliable estimation consistent with established solutions, supporting its validity for practical engineering applications. This consistency further demonstrates the reliability of the RPFEM approach. Unlike nonlinear FEM, which requires iterative stiffness updates, or limit equilibrium methods that rely on empirical assumptions, RPFEM directly evaluates the ultimate load-bearing capacity. Moreover, in contrast to conventional elastoplastic models, RPFEM eliminates uncertainties associated with soil elasticity parameters, providing a more straightforward yet robust framework for assessing failure mechanisms.

***Table 2.** Effect of pile diameter on ultimate lateral resistance p_u*

D (m)	0.4	0.6	1.0	1.5	2.0
p_u	12.25c_u	12.27c_u	12.28c_u	12.28c_u	12.28c_u

Moreover, this study examined the effect of pile diameter on the ultimate lateral resistance of a single pile, with diameters ranging from D=0.4 m to D=2.0 m, as shown in Table 2. The analysis revealed that the ultimate lateral resistance remained nearly constant, between p_u=12.25c_u and p_u=12.28c_u, regardless of the diameter. Interestingly, the RPFEM results indicated that the lateral resistance (p_u) of a single pile, measured per unit length, is largely independent of its diameter. Consequently, since the undrained cohesion strength (c_u) and the pile diameter (D) do not influence the ultimate lateral resistance, the findings confirm that this behavior is consistent across different values of these parameters [11].

3. Analysis of the impact of strength degradation in the soil surrounding piles

During pile installation, driving or boring disturbs the surrounding cohesive soil, remolding particles, increasing pore water pressure, and reducing shear strength, especially within a few pile diameters. The extent of this weakening depends on soil type, installation method, and environmental factors. This study investigates how installation-induced soil degradation affects lateral resistance and pile performance in clayey soils. Accounting for soil strength reduction around the pile improves the accuracy of pile behavior predictions and enhances foundation design reliability.

Therefore, to account for the cohesive strength degradation of the surrounding clayey soil caused by disturbances during pile installation, calculations were performed for cases where the strength c was reduced by 10 kPa - 80 kPa across various degradation widths L (0.1, 0.2, 0.3, 0.4, 0.5 of pile diameter D), as shown in Table 3.

It is estimated that the significant plastic deformation of the soil due to wall friction during pile installation extends approximately several tens of centimeters from the pile wall. Considering pile diameters D=0.6 (m), the above strength degradation ranges were established. The analytical model accounting for the strength degradation is illustrated in Figure 3.

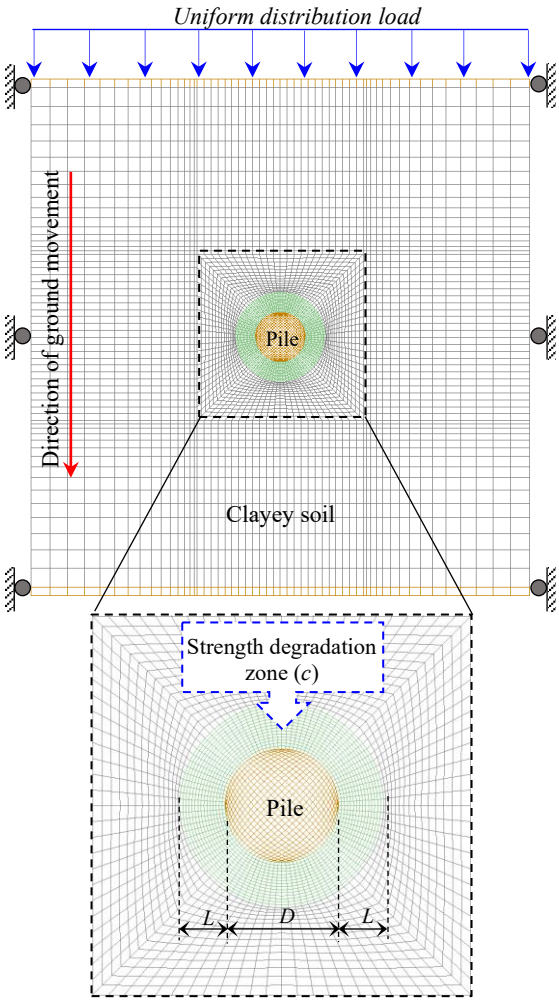

Figure 3. *Model of strength degradation effects in soil surrounding piles with RPFEM.*

Table 3. *Parameters for soil strength degradation around pile*

Cohesive strength degradation c (kPa)	10.0 – 80.0
Degradation width L	0 – 0.5D

The results of the RPFEM analysis, which examines the strength reduction of the surrounding ground due to pile installation, are illustrated in Figure 4. The analysis reveals a distinct trend: as the degradation width L increases, the ultimate lateral resistance consistently decreases across all levels of strength degradation c. This finding underscores the significant impact of surrounding soil conditions on the structural performance of the pile. Specifically, the degradation width L represents the volume of soil that experiences a reduction in strength due to the disturbances associated with pile installation. When the cohesive strength reduction is set at c=40 kPa, it is observed that the ultimate lateral resistance of the single pile decreases sharply, reaching approximately half of its original value, for strength reduction ranges up to L=0.3D. This indicates a significant reduction of the ultimate lateral resistance to the initial strength conditions of the clayey soil.

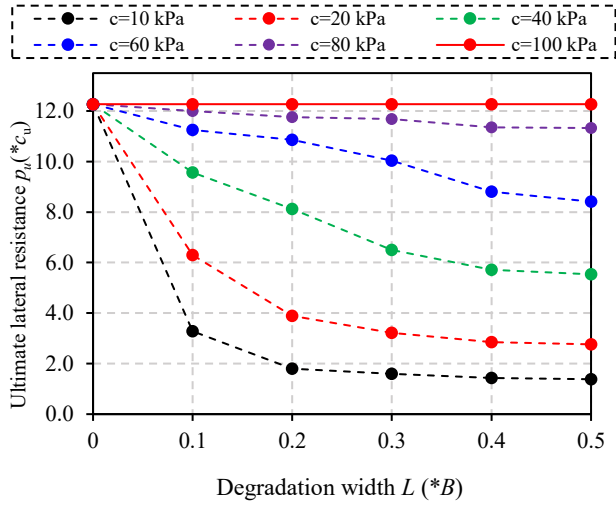

Figure 4. *Ultimate lateral resistance p_u for different degradation widths L, with strength degradation c ranging from c=10 kPa to c=80 kPa*

In all cases of strength reduction, once the degradation width exceeds L=0.3D, the decrease in ultimate lateral resistance (p_u) becomes less pronounced, as shown in Figure 4. This suggests that beyond this threshold, soil exhibits increased stability due to strain hardening or stress redistribution. To capture this trend, the degradation width was analyzed within L=0 – 0.5D. Results show that even as L increases to 2.0D, the decline in p_u continues but at a diminishing rate. This indicates that the most significant impact of degradation width on lateral resistance occurs within the selected range, and further extension would not substantially alter the trend. These findings enhance understanding of soil strength degradation during pile installation and its impact on pile performance limits.

Additionally, Figure 5 presents the deformation diagram and equivalent strain rate contours for the strength degradation case, providing a detailed visualization of deformation patterns and strain rate distribution in the soil surrounding the pile under horizontal movement. The results highlight the spatial variation in soil and pile deformations, demonstrating that lateral pile movement induces the most significant displacements near the pile, with deformation gradually decreasing with distance. These findings align with Komura et al. [29], who reported similar deformation characteristics in laterally loaded piles within degraded soil. The observed correlation underscores the critical role of strength degradation in pile-soil interaction, revealing that weakened soil leads to increased deformation, particularly in regions experiencing severe strength loss. This insight emphasizes the necessity of incorporating degradation effects into pile design to ensure more accurate performance predictions.

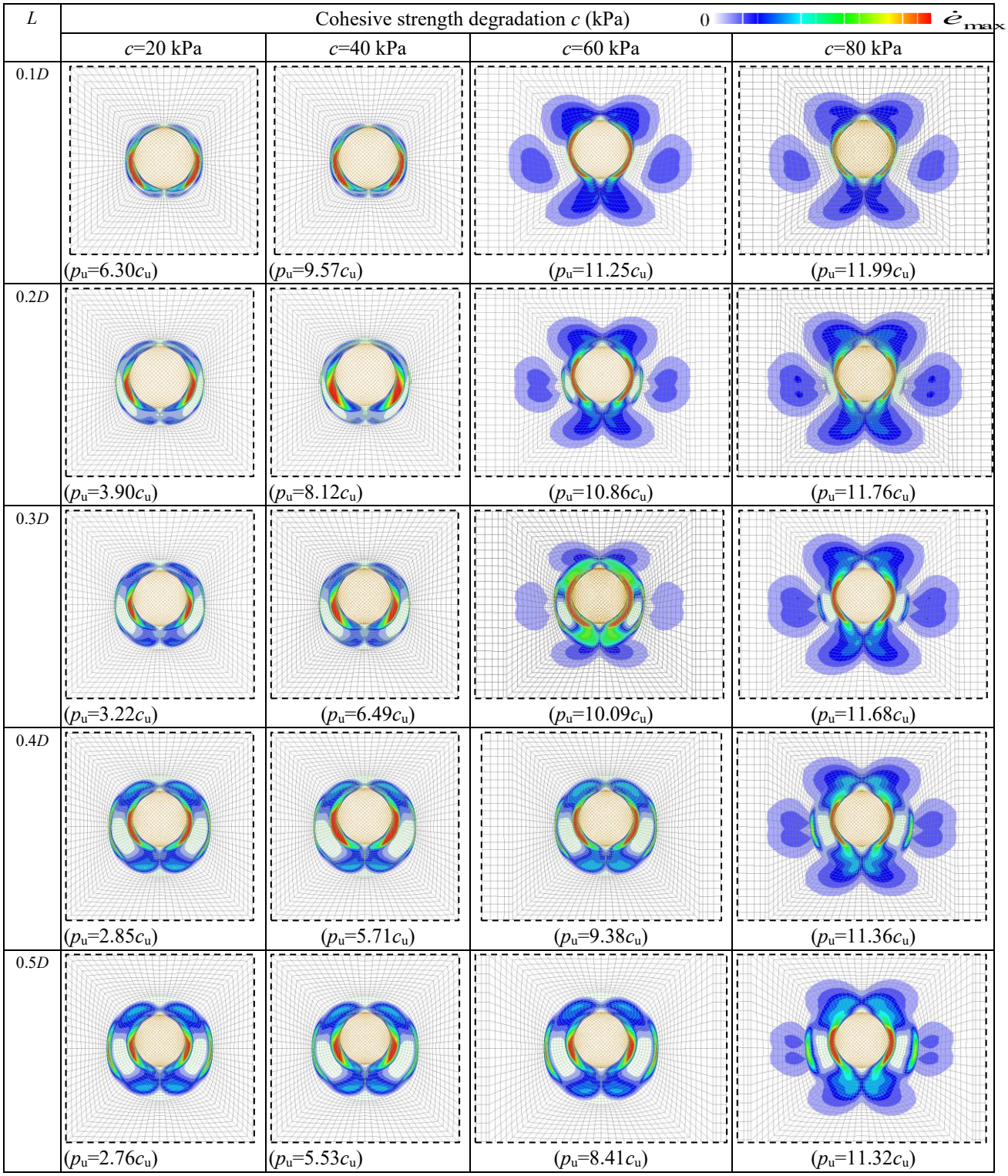

Figure 5. *Failure mechanism of a single pile for varying degradation widths (L), with cohesive strength degradation (c) ranging from 20 kPa to 80 kPa*

From the results obtained using RPFEM, when c=80 kPa, the ultimate lateral resistance p_u remains almost unchanged regardless of the degradation width L. This is because the failure mechanism of the single pile remains largely consistent across different degradation widths, indicating that at higher cohesion values, the impact of soil degradation is minimal.

However, as the cohesive strength c of the clayey soil decreases further, an increase in the degradation width L leads to a substantial reduction in the ultimate lateral resistance of the pile. This occurs because a larger degraded zone weakens a greater portion of the surrounding soil, reducing its ability to resist lateral movement. The loss of cohesive strength in the degraded soil diminishes its capacity to counteract horizontal displacement, thereby providing less support to the pile and significantly reducing its lateral resistance.

To mitigate the adverse effects of soil degradation at lower cohesion values, ground improvement techniques or optimized pile designs should be considered to enhance lateral resistance. Engineers should account for these effects by applying appropriate reduction factors in design calculations and utilizing advanced numerical modeling to predict long-term performance under varying soil degradation cases.

4. Conclusions

The key findings from this study are summarized as follows:

(1) The ultimate lateral resistance of single piles against horizontal ground movement was analyzed using a self-developed Rigid Plastic Finite Element Method (RPFEM). The estimated resistance was approximately $12.27c_u$ in clayey soils, where cu is the undrained shear strength. The failure zone extended $1.5D$ to $2.0D$ from the pile center, consistent with previous studies, confirming the reliability of RPFEM in predicting lateral resistance and failure mechanisms in clayey soils.

(2) This study found that the critical impact of ground strength reduction around piles due to installation effects on the ultimate lateral resistance of a single pile. The analysis shows that such strength degradation significantly reduces the ultimate lateral resistance, with results indicating high sensitivity to changes in surrounding soil strength. These findings emphasize the importance of incorporating installation-induced strength variations into design assessments to ensure more accurate predictions of pile behavior, particularly in sensitive soils.

Acknowledgment: PHAM Ngoc Quang received a Postdoctoral Scholarship with code VINIF.2023.STS.12 from the Vingroup Innovation Foundation (VINIF).

REFERENCES

[1] B. B. Broms, "Lateral Resistance of Piles in Cohesive Soils", *Journal of the Soil Mechanics and Foundations Division, ASCE,* vol. 90, no. 2, pp. 27-63, 1964.

[2] M. F. Randolph, and G. T. Houlsby, "The limiting pressure on a circular pile loaded laterally in cohesive soil", *Géotechnique*, vol. 34, no. 4, pp. 613-623, 1984.

[3] L. T. Chen and H. G. Poulos, "The behavior of piles subjected to lateral soil movements", *Research Report* No. 731, University of Sydney, Australia, 1996.

[4] L. T. Chen and H. G. Poulos, "Piles Subjected to Lateral Soil Movements", *Journal of Geotechnical and Geoenvironmental Engineering, ASCE*, vol. 123, no. 9, pp. 802-811, 1997.

[5] L. T. Chen, H. G. Poulos, and T. S. Hull, "Model test on pile groups subjected to lateral soil movement", *Soils and Foundations*, vol. 37, no. 1, pp. 1-12, 1997.

[6] M. F. Randolph, J. P. Carter, and C. P. Wroth, "Driven piles in clay - The effects of installation and subsequent consolidation", *Géotechnique*, vol. 29, no. 4, pp. 361-393, 1979.

[7] J. K. Mitchell and R. J. Gardner, "In-situ measurement of volume change characteristics of clays", *Journal of the Geotechnical Engineering Division*, vol. 101, no. 4, pp. 403-424, 1975.

[8] D. A. Brown, et al, "Guidelines for use of strain-based methods for the design of driven piles", *Journal of Geotechnical and Geoenvironmental Engineering*, vol. 146 (3), pp. 04020006, 2020.

[9] T. Tamura, S. Kobayashi, and T. Sumi, "Rigid Plastic Finite Element Method for Frictional Materials", *Soils and Foundations*, vol. 27, no. 3, pp. 1-12, 1987.

[10] T. Tamura, S. Kobayashi, and T. Sumi, "Rigid Plastic Finite Element Method in Geotechnical Engineering Computational", *Current Japanese Material Research*, pp. 15-23, 1990.

[11] P. N. Quang, S. Ohtsuka, K. Isobe, and Y. Fukumoto, "Group effect on ultimate lateral resistance of piles against uniform ground movement", *Soils and Foundations*, vol. 59, no. 1, pp. 27-40, 2019.

[12] P. N. Quang, S. Ohtsuka, K. Isobe, Y. Fukumoto, and T. Hoshina, "Ultimate bearing capacity of rigid footing under eccentric vertical load", *Soils and Foundations*, vol. 59, no. 6, pp. 1980-1991, 2019.

[13] P. N. Quang, S. Ohtsuka, K. Isobe, and Y. Fukumoto, "Limit load space of rigid footing under eccentrically inclined load", *Soils and Foundations*, vol. 60, no. 4, pp. 811-824, 2020.

[14] P. N. Quang, "Estimation of Ultimate Lateral Resistance of Pile Group, and Ultimate Bearing Capacity of Rigid Footing under Complex Load by using Rigid Plastic Finite Element Method", 2020. (Doctoral dissertation, Nagaoka University of Technology).

[15] P. N. Quang, and S. Ohtsuka, "Ultimate bearing capacity of rigid footing on two-layered soils of sand–clay", *International Journal of Geomechanics*, vol. 21, no. 7, pp. 04021115, 2021.

[16] P. N. Quang, S. Ohtsuka, K. Isobe, and Y. Fukui, "Consideration on Limit Load Space of Footing on Various Soils Under Eccentric Vertical Load", *in Challenges and Innovations in Geomechanics: Proceedings of the 16th International Conference of IACMAG-Volume 2*, vol. 16, pp. 75-84, 2021. Springer International Publishing.

[17] P. N. Quang, S. Ohtsuka, K. Isobe, and Y. Fukumoto, "Limit load space of rigid strip footing on cohesive-frictional soil subjected to eccentrically inclined loads", *Computers and Geotechnics*, vol. 151, p. 104956, 2022.

[18] N. Q. Pham, and S. Ohtsuka, "Numerical investigation on bearing capacity of rigid footing on sandy soils under eccentrically inclined load", *in Proceedings of the 2nd Vietnam Symposium on Advances in Offshore Engineering: Sustainable Energy and Marine Planning*, pp. 333-341, 2022. Springer Singapore.

[19] P. N. Quang, S. Ohtsuka, K. Isobe, N.V. Pham, and P.H. Hoang, "Limit load space of rigid strip footing on sand slope subjected to combined eccentric and inclined loading", *Computers and Geotechnics*, vol. 162, p. 105652, 2023.

[20] P. N. Vinh, P. N. Quang, and H. Thang, "Effect of foundation surface roughness on ultimate bearing capacity of an eccentrically loaded foundation", *The University of Danang – Journal of Science and Technology*, vol. 21, no. 12.1, pp. 28-33, 2023.

[21] P. N. Quang and P. N. Vinh, "Effect of footing roughness on ultimate bearing capacity of rigid strip footing on sandy soil slope", *the University of Danang – Journal of Science and Technology*, vol. 21, no. 12.1, pp. 22–27, 2023.

[22] P. N. Quang and P. N. Vinh, "Estimation of ultimate bearing capacity of strip footings on cohesive-frictional soils using non-linear shear strength model", The University of Danang – Journal of Science and Technology, vol. 22, no. 6.A, pp. 29-34, 2024.

[23] P P. N. Quang, S. Ohtsuka, K. Isobe, P. N. Vinh, and H. P. Hoa, "Undrained failure envelope (*V–H–M*) of rigid strip footings on clayey soil slopes under eccentric and inclined loads", *Arabian Journal for Science and Engineering*, vol. 50, pp. 1–28, 2025.

[24] P. N. Quang and P. N. Vinh, "Safety factor analysis of natural slopes using Rigid Plastic Finite Element Method (RPFEM)", *The University of Danang – Journal of Science and Technology*, vol. 22, no. 12, pp. 49-54, 2024.

[25] K. Georgiadis, S. W. Sloan, and A. V. Lyamin, "Ultimate lateral pressure of two side-by-side piles in clay", *Géotechnique*, vol. 63, no. 9, pp. 733-745, 2013.

[26] K. Georgiadis, S. W. Sloan, and A. V. Lyamin, "Effect of loading direction on the ultimate lateral soil pressure of two piles in clay", *Géotechnique*, vol. 63, no. 13, pp. 1170-1175, 2013.

[27] K. Georgiadis, S. W. Sloan, and A. V. Lyamin, "Undrained limiting lateral soil pressure on a row of piles", *Computer and Geotechnics*, vol. 54, pp. 175-184, 2013.

[28] Z. Zhao, D. Li, F. Zhang, and Y. Qiu. "Ultimate lateral bearing capacity of tetrapod jacket foundation in clay", *Computers and Geotechnics*, vol. 84, pp. 164-173, 2017.

[29] S. Koumura, Y. Shiratori, S. Ohtsuka, and T. Hoshina, "Estimation of ultimate lateral resistance of pile in clayey ground," *Proc. 14th Int. Conf. IACMAG 2014*, Taylor & Francis, pp. 947-950, 2015.